AIMS Energy, 6 (5): 695–709.
DOI: 10.3934/energy.2018.5.695
Received: 13 June 2018
Accepted: 03 September 2018
Published: 07 September 2018

http://www.aimspress.com/journal/energy

Research article

Fuzzy PI controller for bidirectional power flow applications with harmonic current mitigation under unbalanced scenario

Nagaraj C[1,*] and K Manjunatha Sharma[2]

[1] Research Scholar, Department of Electrical & Electronics Engineering, National Institute of Technology Karnataka (NITK), Surathkal, P.O. 575025, India
[2] Associate Professor, Department of Electrical & Electronics Engineering, National Institute of Technology Karnataka (NITK), Surathkal, P.O. 575025, India

*** Correspondence:** Email: assiniraj@gmail.com; Tel: +919916444330.

Abstract: The depletion of fossil fuels and environmental concern forces the extraction of power from low carbon fuels causes generation problem due to intermittent solar-wind renewable energy sources and power electronic applications. Furthermore, the significant amount of non-linear loads in the system causes power quality problems. Nowadays, the more and more DC loads like LED lights to save energy consumption are connected to the AC distribution system. These DC loads are connected at DC grid side in order to avoid the extra AC/DC power conversion loss. In this paper, the proposed d-q reference current method applied for shunt active power filter based 3-phase 4-leg bidirectional interfacing converter with fuzzy PI controller to achieve the real power transfer between DC grid side and AC grid side with current harmonics compensation at common connecting point simultaneously under balanced and unbalanced distorted grid and non-linear load conditions. The hysteresis current control comparator without PLL is used to compare actual grid current with reference filter current and generate the switching pulses for driving the bidirectional interfacing converter. The DC grid shunt connected intermittent hybrid solar-wind energy sources are integrating with AC grid utility through bidirectional interfacing converter has been into consideration for simulation studies. The MATLAB/SIMULINK tool is used to yield the improved grid current THD with fuzzy logic controller over PI controller.

Keywords: bidirectional interlinking converter; common connecting point; hysteresis current control; hybrid solar-wind energy sources; i_d-i_q method

1. Introduction

Power generation by renewable energy sources is the most economical one to provide continuous power to the consumer end at the level of distribution system. Due to more and more non-linear loads and power electronic devices, the power quality issues arises in the system. The study of these issues for distinct network configuration is to build appropriate controller to the power converters accordingly in order to supply quality power at the end users in both grid connected and isolated mode [1,2].

The alternative control strategy based shunt active power filter (SAPF) is presented to improve the suppression of harmonic efficiency as well as disturbance caused by unbalanced non-linear loads under unbalanced distorted grid voltage condition [3]. The proposed controller of SAPF based voltage source inverter (VSI) is to address the DG with grid connected issues under balanced undistorted grid with unbalanced non-linear load [4]. The proposed predictive controller for SAPF based 4-leg VSI is analyzed under balanced grid with unbalanced load to compensate unbalanced load current obtained from 1-phase non-linear load, compensation of current harmonics at common connecting point (CCP) and reactive power simultaneously [5].

A direct power control scheme of SAPF based 3-phase 3-leg VSI is proposed with utilization of high selectivity filter instead of classical low pass filter. This allows to control real and reactive power directly injected by SAPF to the AC grid side without using phase locked loop (PLL) and current control loops under any supply voltage conditions [6]. The advanced current controller in d-q frame using combination of PI and repetitive control is presented over traditional current controller with PI control. This method improves the harmonic current compensation irrespective of reduced number of current sensors under source voltage distortion [7]. The optimization algorithm is developed to regulate 4-leg VSI SAPF in order to perform harmonic currents compensation, power factor correction under distorted supply voltage condition. This technique also solved mathematically using Lagrangian formulation and has fast dynamic response [8]. The controller scheme based on Lyapunov control theory is developed for stable operation of SAPF with grid connected mode. This method done the analysis of improvement in harmonic currents compensation, active and reactive power sharing at the same time [9]. The I cosine ANFIS control based dynamic SAPF is presented effectively to enhance the power quality at AC grid source along with real and reactive power sharing with close to unity power factor [10].

In the above papers, the application of SAPF based converter controller are discussed only for DC-AC unidirectional power flow applications with power quality improvement. Also, the PLL used for grid synchronization which creates difficulty in case of unbalanced grid distorted conditions. Nowadays, the more and more DC loads like LED lights to save energy consumption are connected to the AC distribution system. These DC loads are connected at DC grid side in order to eliminate the extra AC/DC power conversion loss. Therefore, in this paper, the DC-AC/AC-DC bidirectional power flow applications with power quality improvement are discussed. The main objective of this study is to eliminate the AC-DC conversion stage and PLL for the cost effective system. The AC-DC conversion stage is eliminated by placing the DC load at DC grid side and making the 3-phase converter as bi-directional. Further, PLL is eliminated in order to avoid the grid synchronization problem during unbalanced distorted grid conditions. The proposed d-q reference current control technique applied to the SAPF based 3-phase 4-leg bidirectional interfacing converter (BIC) with fuzzy logic controller (FLC) resulted in improved power quality performance over PI controller.

Further, the proposed system also resulted in effective real power transfer between DC grid and AC grid side, current harmonics compensation at CCP, power factor compensation and load neutral current compensation. The hysteresis current control (HCC) comparator without PLL is used to generate the switching pulses for driving the gate of BIC. The MATLAB/SIMULINK tool is carried out for balanced and unbalanced distorted grid and non-linear load conditions.

2. System configuration

Figure 1 shows a block diagram of grid interfacing DC shunted intermittent hybrid solar-wind energy system (HSWES) via BIC in which shunted 48 kW PV array designed at 1000 W/m^2 and 100 kW variable speed PMSG wind turbine designed at rated 12 m/s wind speed which is rectified with unregulated rectifier from AC to DC output power, DC-DC converter and variable DC resistive load are connected to DC grid side whereas unbalanced variable AC non-linear RL load is connected to AC grid side.

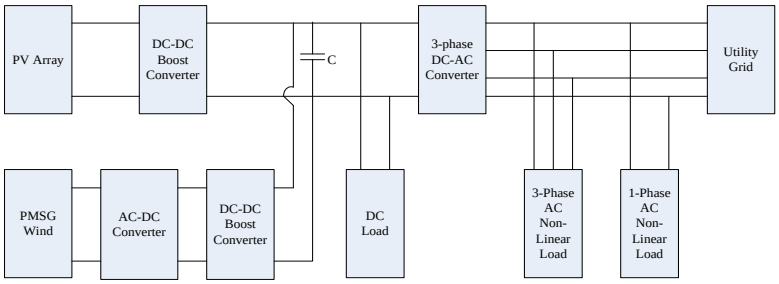

Figure 1. Block diagram of grid connected HSWES.

2.1. Modeling of PV array

The output current of the PV array is modeled by the following mathematical equations and the modeling parameters for PV array are tabulated in Table 1.

$$I_m = I_{pv}N_{pp} - I_o N_{pp}\left[exp\left(\frac{V+R_s\left(\frac{N_{ss}}{N_{pp}}\right)I}{V_t a N_{ss}}\right) - 1\right] \tag{1}$$

where, I_{pv}—photo current which varies continuously depends on the intermittent irradiation level and temperature as follows,

$$I_{pv} = \left(I_{pv,n} + K_i \Delta T\right)\frac{G}{G_n} \tag{2}$$

V_t—thermal voltage junction is given by,

$$V_t = \frac{KTN_s}{q} \tag{3}$$

$I_{pv,n}$—photo current generated at actual condition as follows,

$$I_{pv,n} = \left(R_p + R_s\right)\frac{I_{sc,n}}{R_p} \tag{4}$$

ΔT—change in actual and reference temperature as follows,

$$\Delta T = \left(T - T_{ref}\right) \tag{5}$$

I_0—diode saturation current depends on temperature as follows,

$$I_o = \frac{I_{sc}+K_i\Delta T}{exp\left(\frac{V_{oc,n}+K_v\Delta T}{aV_t}\right)-1} \tag{6}$$

Table 1. Parameters for PV array model [11,12].

Parameters	**Values**
Short circuit current	I_{sc} = 3.87 A
Open circuit voltage	V_{oc} = 42.1 V
No. of series cells	N_s = 72
No. of series string modules	N_{ss} = 20
No. of parallel string modules	N_{pp} = 20
Ideality factor	a = 1.3997
Boltzmann constant	K = 1.38e^{-23} J/K
Electron charge	q = 1.602e^{-19} C
Current temperature coefficient	K_i = 3.2e^{-03} A/K
Voltage temperature coefficient	K_v = −0.1230 V/K
Reference temperature	T_{ref} = 298.15 K
Nominal temperature	T= 298.15 K

2.2. Modeling of PMSG variable wind speed

The modeling parameters for variable speed PMSG wind are tabulated in Table 2 and the aerodynamic power obtained from wind turbine depends on wind speed is expressed by,

$$P_m = 0.5\rho V_w^3 A C_p(\lambda,\beta) \tag{7}$$

The power coefficient, C_p (λ, β) decides the total power available from wind and is given by,

$$C_p(\lambda,\beta) = 0.5176\left(\frac{116}{\lambda_i} - 0.4\beta - 5\right)exp^{\frac{-21}{\lambda_i}} \tag{8}$$

Tip speed ratio,

$$\lambda = \frac{\omega_m R}{V_w} \tag{9}$$

$$\lambda_i = \left[\frac{1}{\lambda+0.08\beta} - \frac{0.035}{\beta^3+1}\right]^{-1} \tag{10}$$

Blade pitch angle,

$$\beta = \frac{1}{\frac{1}{\lambda+0.08\theta} - \frac{0.035}{\theta^3+1}} \tag{11}$$

The function of β is to control the input mechanical power of wind turbine generator at high wind speed.

The PMSG model in dq frame is given by,

$$\frac{di_{ds}}{dt} = \frac{1}{L_d}\left[-V_{ds} - R_s i_{ds} + \omega L_q i_{qs}\right] \tag{12}$$

$$\frac{di_{qs}}{dt} = \frac{1}{L_q}\left[-V_{qs} - R_s i_{qs} - \omega L_d i_{ds} + \omega \phi_m\right] \tag{13}$$

If the rotor is cylindrical $L_d = L_q = L_s$, the electromagnetic torque is,

$$T_e = 1.5 P \phi_m i_{qs} \tag{14}$$

Table 2. Parameters for PMSG wind model [13].

Parameters	Values
Stator phase resistance	2.875 Ω
d & q-axis phase inductance	8.5 m H
Inertia	$0.8e^{-03}$ kg-m^2
Torque constant	12 N-m/A peak
No. of pole pairs	8
Wind power output	100 kW
Rated wind speed	12 m/s

3. Control methods

The overall control diagram of the proposed system is depicted in Figure 2 and discussed in this section.

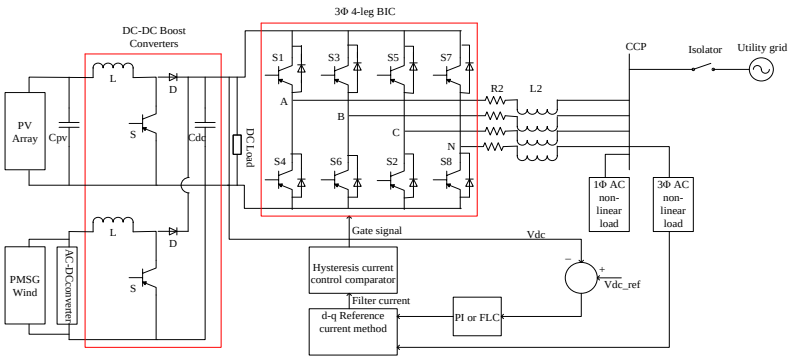

Figure 2. Overall control diagram of the proposed system.

3.1. d-q reference current method

The control diagram of d-q reference current method is shown in detail in Figure 3. The determination of angle θ with respect to α-β frame is obtained by d-q frame. The transformation of d-q reference frame is illustrated as,

$$\begin{bmatrix} i_d \\ i_q \\ i_o \end{bmatrix} = \begin{bmatrix} cos\theta & sin\theta & 0 \\ -sin\theta & cos\theta & 0 \\ 0 & 0 & 1 \end{bmatrix} \begin{bmatrix} i_\alpha \\ i_\beta \\ i_o \end{bmatrix} \tag{15}$$

The above each current has DC average value and AC oscillating value,

$$i_d = \bar{\imath}_d + \tilde{\imath}_d \tag{16}$$

$$i_q = \bar{\imath}_q + \tilde{\imath}_q \tag{17}$$

In the above equations, only the magnitude of currents is transformed and power calculations are performed on d-q-axis components. The zero sequence current components remain unchanged when the d-axis has same direction as like voltage space vector $\overline{v}$. Hence,

$$\begin{bmatrix} i_d \\ i_q \\ i_o \end{bmatrix} = \frac{1}{v_{\alpha\beta}} \begin{bmatrix} v_\alpha & v_\beta & 0 \\ -v_\beta & v_\alpha & 0 \\ 0 & 0 & v_{\alpha\beta} \end{bmatrix} \begin{bmatrix} i_{L\alpha} \\ i_{L\beta} \\ i_{Lo} \end{bmatrix} \tag{18}$$

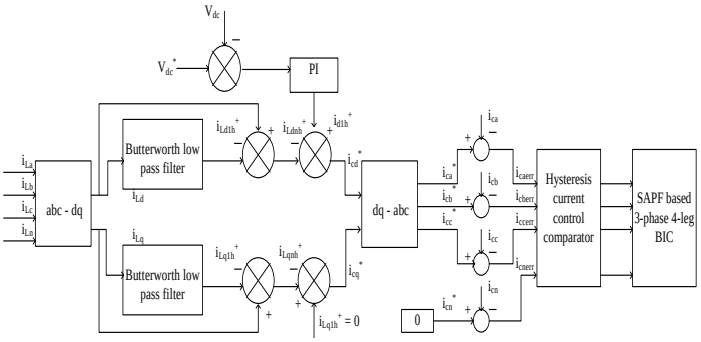

Figure 3. d-q reference current method.

The reference supply current will be determined as follows,

$$i_{sd} = \bar{\imath}_{Ld}; i_{sq} = i_{so} = 0 \tag{19}$$

$$i_{Ld} = \frac{v_\alpha i_{L\alpha} + v_\beta i_{L\beta}}{v_{\alpha\beta}} = \frac{P_{\alpha\beta}}{\sqrt{v_\alpha^2 + v_\beta^2}} \tag{20}$$

The DC average value of Eq 20 is,

$$\bar{\imath}_{Ld} = \left(\frac{P_{L\alpha\beta}}{v_{\alpha\beta}}\right)_{dc} = \left(\frac{P_{L\alpha\beta}}{\sqrt{v_\alpha^2 + v_\beta^2}}\right)_{dc} \tag{21}$$

Multiplying Eq 20 with unit vector because of reference supply current in phase with voltage at CCP,

$$i_{sref} = \bar{\imath}_{Ld} \frac{1}{v_{\alpha\beta}} \begin{bmatrix} v_\alpha \\ v_\beta \\ 0 \end{bmatrix} \tag{22}$$

$$\begin{bmatrix} i_{s\alpha ref} \\ i_{s\beta ref} \\ i_{soref} \end{bmatrix} = \left(\frac{P_{L\alpha\beta}}{v_{\alpha\beta}}\right)_{dc} \frac{1}{v_{\alpha\beta}} \begin{bmatrix} v_\alpha \\ v_\beta \\ v_o \end{bmatrix} \tag{23}$$

$$\begin{bmatrix} i_{s\alpha ref} \\ i_{s\beta ref} \\ i_{soref} \end{bmatrix} = \left(\frac{P_{L\alpha\beta}}{\sqrt{v_\alpha^2+v_\beta^2}}\right)_{dc} \frac{1}{\sqrt{v_\alpha^2+v_\beta^2}} \begin{bmatrix} v_\alpha \\ v_\beta \\ v_o \end{bmatrix} \tag{24}$$

The main benefits of this d-q scheme are that the angle θ is determined directly from grid source voltage without using PLL to synchronize with utility grid. The PI control is applied to the d-axis in d-q reference frame to control the small real component current and then the current controller controls this current to regulate the DC link voltage constant across capacitor.

Figure 4 represents a process of DC voltage regulation with FLC. It comprises of mainly three blocks, first one is fuzzification using "continuous universe of discourse", second one is inference mechanism based on "fuzzy implication using mamdani's operator" and the third one is defuzzification using "centroid method".

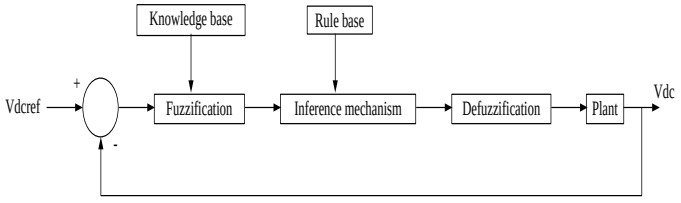

Figure 4. DC voltage regulation with FLC [14].

The FLC was designed with triangular membership function (TMF) due to low computation time. The TMF of 3 × 3 or 5 × 5 is not able to maintain DC link voltage constant and creates an error voltage due to voltage difference. In order to avoid such difficulties, we have considered 7 × 7 TMF to optimize the error efficiently which gives best results in terms of current harmonic filtering under steady and transient state conditions. The development of FLC algorithm is with two inputs and one output each having "seven fuzzy sets". Firstly, the input error "e" and change in error "ce" have been placed of the angular speed to be the input variables of FLC as shown in Figure 5. Then the output variable of FLC is given by the current control "I_{max}" as shown in Figure 6. These numerical variables are converted into linguistic variables and the fuzzy rule mechanism are constructed in Table 3.

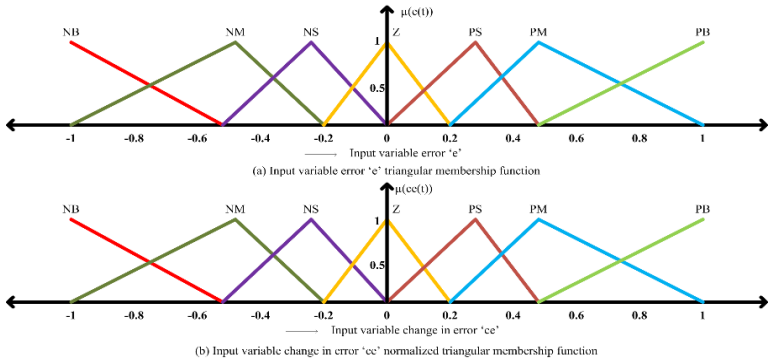

Figure 5. Input variables "e" and "ce" of FLC [14].

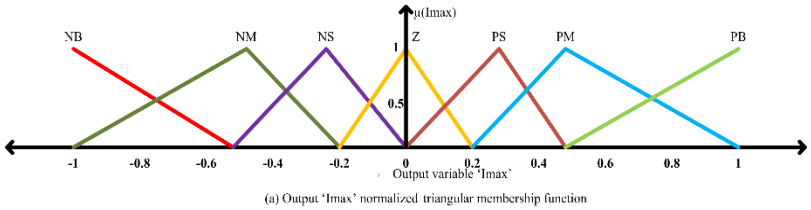

Figure 6. Output variables "I_{max}" of FLC [14].

Table 3. Fuzzy rule mechanism [14].

e ce	NB	NM	NS	Z	PS	PM	PB
NB	NB	NB	NB	NB	NM	NS	Z
NM	NB	NB	NB	NM	NS	Z	PS
NS	NB	NB	NM	NS	Z	PS	PM
Z	NB	NM	NS	Z	PS	PM	PB
PS	NM	NS	Z	PS	PM	PB	PB
PM	NS	Z	PS	PM	PB	PB	PB
PB	Z	PS	PM	PB	PB	PB	PB

3.2. Hysteresis current control comparator

The transfer of real power between AC-DC buses with utility grid depends on DC link voltage control. The working of HCC comparator without PLL as compared to HCC comparator with PLL [3] is discussed as follows.

The reference signals i_{ca}^*, i_{cb}^*, i_{cc}^* and i_{cn}^* obtained from d-q method are compared with actual grid currents i_{ca}, i_{cb}, i_{cc} and i_{cn} as shown below to get the current errors which is given to the HCC comparator to generate the switching pulses (P_1 to P_8) for driving the BIC.

$$\begin{aligned} i_{caerr} &= i_{ca}^* - i_{ca} \\ i_{cberr} &= i_{cb}^* - i_{cb} \\ i_{ccerr} &= i_{cc}^* - i_{cc} \\ i_{cnerr} &= i_{cn}^* - i_{cn} \end{aligned} \tag{25}$$

If the current errors are above the upper bandwidth, then the upper switch of the corresponding phase leg is turned OFF whereas if not, then the upper switch is turned ON and vice-versa. This HCC comparator without PLL has very rapid response and good accuracy due to sudden change of load and its control diagram is depicted in Figure 7.

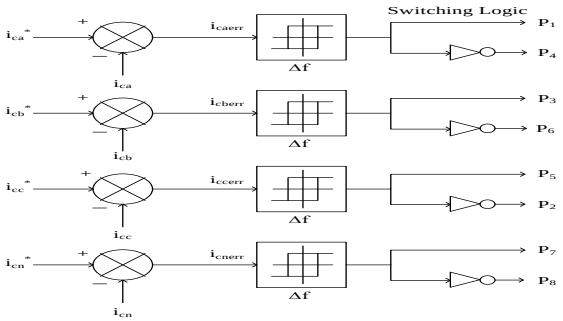

Figure 7. Control diagram of HCC.

4. Case study: Results and discussion for HSWES

The case study results for the given system shown in Figure 2 are simulated using MATLAB/SIMULINK tool under different grid and non-linear load conditions and the parameters used for simulation is tabulated in Table 4.

Table 4. Parameters used for simulation.

Parameters	Values
Grid voltage	V = 400 V
Grid frequency	f = 50 Hz
Grid resistance	R_2 = 0.1 Ω
Grid inductance	L_2 = 0.01 mH
DC link capacitor	C_{dc} = 7000 μF
DC link voltage	V_{dc} = 800 V

4.1. Performance of d-q method with comparison of PI & FLC under balanced undistorted grid & balanced non-linear load condition at solar irradiation, I_{rr} = 200 W/m^2 & wind speed, w_s = 8 m/s in winter

In this case, the performance of the overall system is analyzed with balanced undistorted grid and balanced non-linear load conditions. The overall system main grid voltage with PI control is shown in Figure 8a and fuzzy control is shown in Figure 8b. Initially, before applying the d-q reference current control to the BIC, the grid current is similar to the load current with both PI and FLC (Figure 8i,j). After applying the d-q reference current control to the BIC, the extraction of reference currents is compared with the actual currents by HCC. The DC link voltage regulates constant with the PI controller (Figure 8g) and FLC (Figure 8h), which plays a main role in transferring the power between AC-DC buses. Further, the polluted grid current starts to filter out to become almost sinusoidal is shown in Figure 8c with PI and Figure 8d with FLC and the

corresponding grid current THD after filtering is shown in Figure 8k with PI, 1.94% and Figure 8l with FLC, 1.59% respectively.

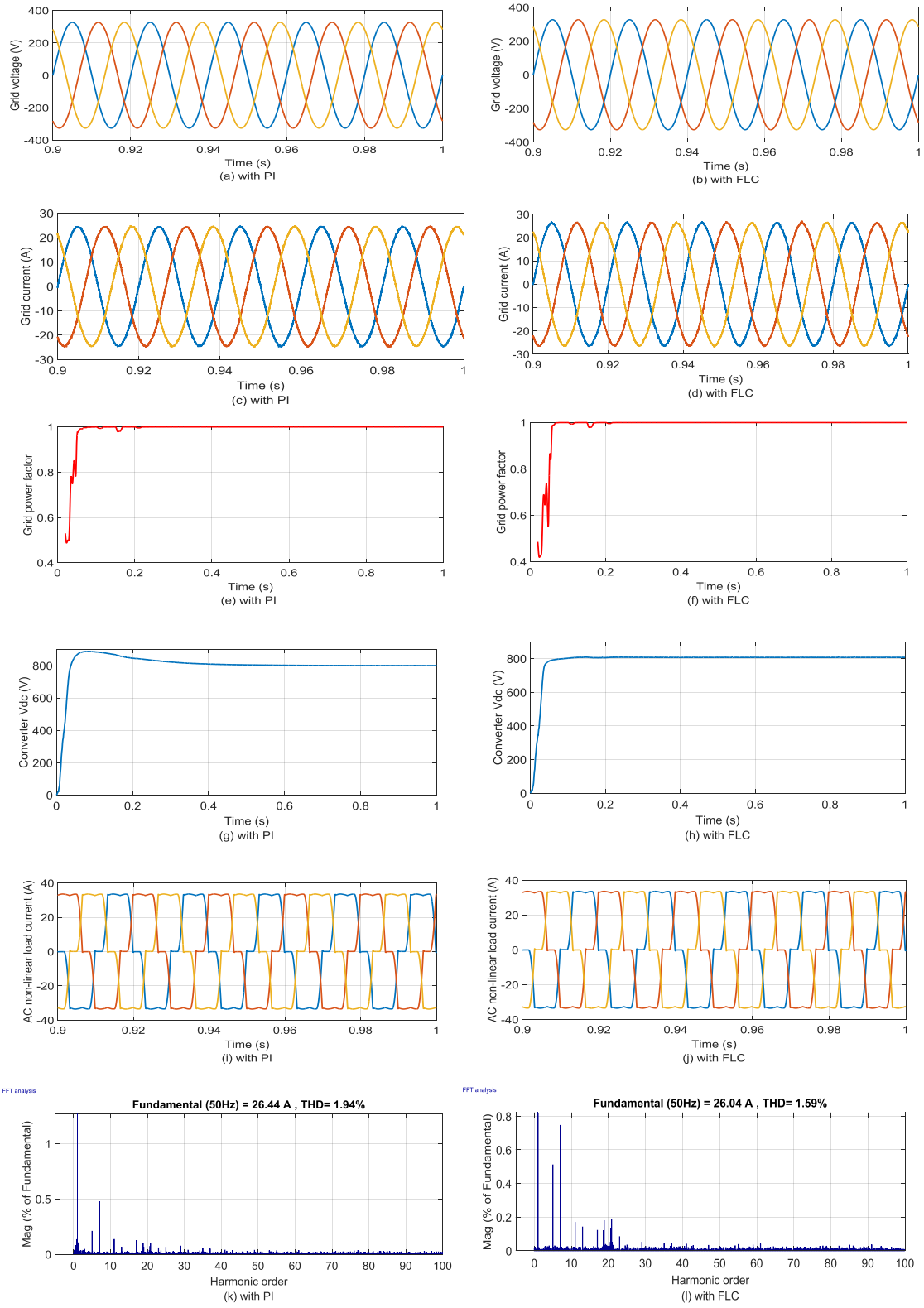

Figure 8. (a) & (b) Grid voltage, (c) & (d) Grid current, (e) & (f) Grid power factor, (g) & (h) Converter V_{dc}, (i) & (j) AC non-linear load current and (k) & (l) Grid THD current.

With both PI and FLC, the power generated by PMSG wind, P_{wind} = 61 kW at 8 m/s and PV array, P_{pv} = 8 kW at 200 W/m^2 in winter. At DC grid side, the HSWES are generating power more than the DC load demand, P_{dcload} = 64 kW. Thus, the remaining surplus power from HSWES is transferring from DC bus to AC bus through BIC, which acts an inverter, P_{conv} = 5 kW (Figure 9b). At AC grid side, the AC load, P_{acload} = 17 kW have been drawn the power from both grid, P_{grid} = 12 kW with Q_{grid} = 0 kW and HSWES through BIC, P_{conv} = 5 kW to meet its demand (Figure 9a). The Q_{grid} indicates that the power factor becomes almost +ve UPF due to grid is supplying the power, which can be observed in Figure 8e, f.

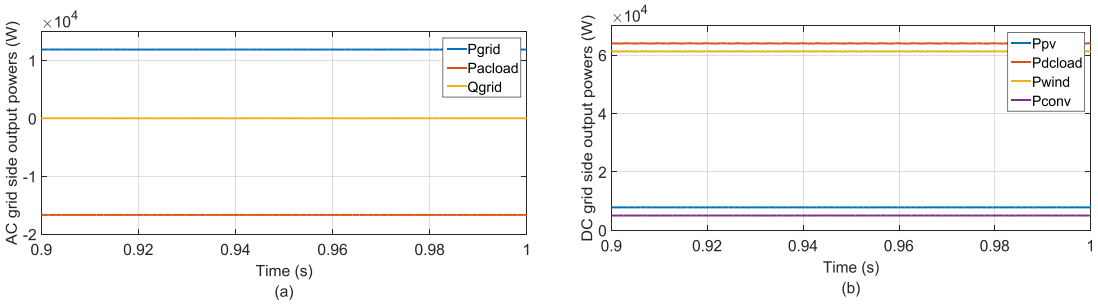

Figure 9. (a) AC grid side output powers and (b) DC grid side output powers.

4.2. Performance of d-q method with comparison of PI & FLC under unbalanced distorted grid & unbalanced non-linear load condition at solar irradiation, I_{rr} = 800 W/m^2 & wind speed, w_s = 2 m/s in summer

In this case, the overall system performance is analyzed with unbalanced distorted grid and unbalanced non-linear load conditions. Figure 10a with PI and Figure 10b with FLC presents the main grid voltage of the system. Initially, before connecting BIC to the network, the grid current is similar to the load current with both PI and FLC (Figure 10i,j). After connecting BIC to the network, the reference currents extract from the d-q method and these currents are compared with the actual currents by HCC. The DC link voltage regulates constant with the PI controller (Figure 10g) the FLC (Figure 10h), which plays a main role in transferring the power between AC-DC buses. Further, the polluted grid current starts to filter out to become almost sinusoidal is shown in Figure 10c with PI and Figure 10d with FLC and the corresponding grid current THD after filtering is shown in Figure 10k with PI, 1.62% and Figure 10l with FLC, 1.30% respectively.

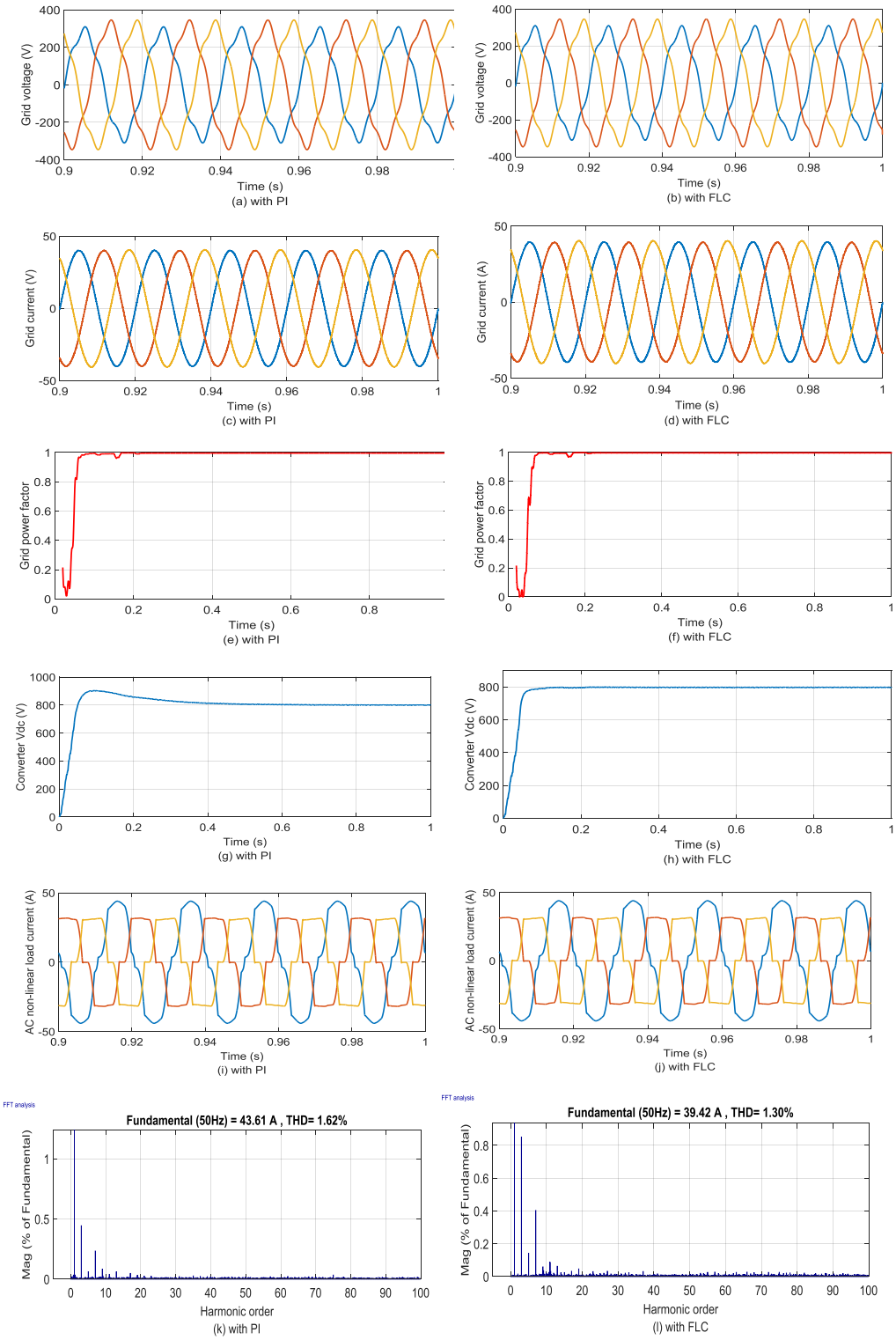

Figure 10. (a) & (b) Grid voltage, (c) & (d) Grid current, (e) & (f) Grid power factor, (g) & (h) Converter V_{dc}, (i) & (j) AC non-linear load current and (k) & (l) Grid THD current.

With both PI and FLC, the power generated by PMSG wind, P_{wind} = 5.5 kW at 2 m/s and PV array, P_{pv} = 38 kW at 800 W/m^2 in summer. On DC grid side, the generation of HSWES are less than the DC load demand, P_{dcload} = 46 kW. To satisfy the DC load demand, the remaining power drawn

from the grid is transferring from AC bus to DC bus through BIC, which acts a rectifier, P_{conv} = 2.5 kW (Figure 11b). On AC grid side, the AC load, P_{acload} = 16 kW have been drawn the power from only grid, P_{grid} = 18.5 kW with Q_{grid} = 0 kW through BIC, P_{conv} = 2.5 kW to meet its demand (Figure 11a). The Q_{grid} indicates that the power factor becomes almost +ve UPF due to grid is supplying the power, which can be observed in Figures 10e, f.

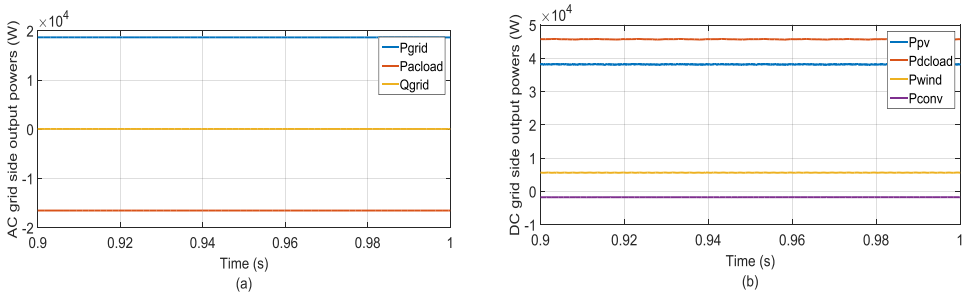

Figure 11. (a) AC grid side output powers and (b) DC grid side output powers.

With both PI and FLC, in case of unbalanced non-linear load on AC grid side, the filter current flows to the CCP through the 4th leg of BIC for compensation of neutral load current as depicted in Figure 12. In both case 4.1 and 4.2, the grid current THD is improved with FLC over PI controller is depicted in Table 5. Thus, the obtained results conclude that the performance of d-q method with FLC holds good over PI controller.

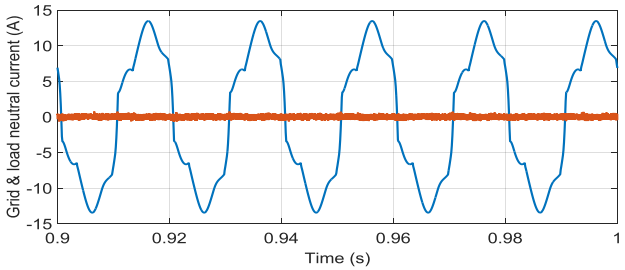

Figure 12. Grid & load neutral current.

Table 5. Power quality improved with FLC over PI controller.

Gird condition	Non-linear load condition	Case	Grid current THD (%)	
			PI Controller	Fuzzy Logic Controller
Balanced Undistorted	Balanced	4.1	1.94	1.59
Unbalanced Distorted	Unbalanced	4.2	1.62	1.30

5. Conclusions

In this paper, the AC-DC conversion stage and PLL has been eliminated in the grid connected HSWES resulted in cost effective system. The BIC has been used to eliminate the extra AC-DC

conversion stage. Further, PLL has been eliminated in order to avoid the grid synchronization problem during distorted grid conditions. The proposed d-q reference current control technique using fuzzy PI controller has been applied to SAPF based 3-phase 4-leg BIC. Also, the HCC comparator without PLL has been employed to give the switching pulses to drive the BIC. The extensive simulation analysis has been carried out in MATLAB/SIMULINK tool for balanced and unbalanced distorted grid and non-linear load conditions. For the different case studies, the proposed d-q reference current control technique with FLC resulted in improved power quality performance over PI controller. Further, the proposed system also resulted in effective real power transfer between DC grid and AC grid side, current harmonics compensation at CCP, power factor compensation and load neutral current compensation.

Conflict of interest

All authors declare no conflicts of interest in this paper.

References

1. Arul PG, Ramachandaramurthy VK, Rajkumar RK (2015) Control strategies for a hybrid renewable energy system: A review. *Renew Sust Energ Rev* 42: 597–608.
2. Ullah W, Mekhilef M, Seyedmahmoudian M, et al. (2017) Active power filter (APF) for mitigation of power quality issues in grid integration of wind and photovoltaic energy conversion system. *Renew Sust Energ Rev* 70: 635–655.
3. Özerdem ÖC, Khadem SK, Biricik S, et al. (2014) Real-time control of shunt active power filter under distorted grid voltage and unbalanced load condition using self-tuning filter. *IET Power Electron* 7: 1895–1905.
4. Pouresmaeil E, Akorede MF, Montesinos-Miracle D, et al. (2014) Hysteresis current control technique of VSI for compensation of grid-connected unbalanced loads. *Electr Eng* 96: 27–35.
5. Acuna P, Moran L, Rivera M, et al. (2014) Improved active power filter performance for renewable power generation systems. *IEEE T Power Electron* 29: 687–694.
6. Mesbahi N, Ouari A, Abdeslam DO, et al. (2014) Direct power control of shunt active filter using high selectivity filter (HSF) under distorted or unbalanced conditions. *Electr Power Syst Res* 108: 113–123.
7. Trinh QN, Lee HH (2014) An enhanced grid current compensator for grid-connected distributed generation under nonlinear loads and grid voltage distortions. *IEEE T Ind Electron* 61: 6528–6537.
8. Kanjiya P, Khadkikar V, Zeineldin HH (2015) Optimal control of shunt active power filter to meet IEEE Std. 519 current harmonic constraints under nonideal supply condition. *IEEE T Ind Electron* 62: 724–734.
9. Mehrasa M, Pouresmaeil E, Zabihi S, et al. (2016) A control strategy for the stable operation of shunt active power filters in power grids. *Energy* 96: 325–334.
10. Kasa S, Ramanathan P, Ramasamy S, et al. (2016) Effective grid interfaced renewable sources with power quality improvement using dynamic active power filter. *Int J Electr Power Energy Syst* 82: 150–160.

11. Villalva MG, Gazoli JR, Filho ER, et al. (2009) Comprehensive Approach to Modeling and Simulation of Photovoltaic Arrays. *IEEE T Power Electron* 24: 1198–1208.
12. Rakotomananandro FF (2011) Study of Photovoltaic System. Master of Science. The Ohio State University.
13. Jayalakshmi NS, Gaonkar DN, Kumar KSK (2012) Dynamic modeling and performance analysis of grid connected PMSG based variable speed wind turbines with simple power conditioning system. *IEEE Int Conf Power Electron* 2013: 1–5.
14. Ouchen S, Betka A, Abdeddaim S, et al. (2016) Fuzzy-predictive direct power control implementation of a grid connected photovoltaic system, associated with an active power filter. *Energy Convers Manag* 122: 515–525.

AIMS Press